Proceedings of the ASME 2010 International Design Engineering Technical Conferences & Computers and Information in Engineering Conference
IDETC/CIE 2010
August 15-18, 2010, Montreal, Quebec, Canada

DETC2010-28863

A CABLE-ACTUATED ROBOTIC LUMBAR SPINE FOR PALPATORY TRAINING OF MEDICAL STUDENTS

Ernur Karadogan and **Robert L. Williams II**
Mechanical Engineering, Ohio University
Athens, Ohio, USA
williar4@ohio.edu

ABSTRACT

This paper presents the kinematic and pseudostatic analyses of a fully cable-actuated robotic lumbar spine (RLS) which can mimic in vivo human lumbar spine movements to provide better hands-on training for medical students. The design incorporates five active lumbar vertebrae between the first lumbar vertebra and the sacrum, with dimensions of an average adult human spine. Medical schools can benefit from a tool, system, or method that will help instructors train students and assess their tactile proficiency throughout their education. The robotic lumbar spine has the potential to satisfy these needs in palpatory diagnosis. Medical students will be given the opportunity to examine their own patient that can be programmed with many dysfunctions related to the lumbar spine before they start their professional lives as doctors. The robotic lumbar spine can be used to teach and test medical students in their capacity to be able to recognize normal and abnormal movement patterns of the human lumbar spine under flexion-extension and lateral bending. This project focus is on palpation, but the spine robot could also benefit surgery training/planning and other related biomedical applications.

KEYWORDS

Cable-actuated robot, robotic lumbar spine, RLS, palpatory training

1. INTRODUCTION

Today, in most medical schools, the art of palpation is usually taught by using voluntary human patients who are mostly palpated by the instructor for demonstrative purposes. Meanwhile, the students usually watch the process and get to palpate only their lab partners as "patients" who are, considering the general population of medical students, relatively young and healthy (many with limited dysfunctions). It is, however, very difficult to be able to find and demonstrate a different patient for every single dysfunction that the students are taught during the lectures or in the laboratories. Therefore, it is still hard to teach and learn palpatory diagnosis for different variations of dysfunctions. The lack of a means for evaluating the transfer of practical information from the instructor to the students is another drawback that the medical schools are facing today. There exists no assessment device for instructors to objectively evaluate progress and success of the students in real-life situations.

The need for a "gold standard" to objectively assess the palpation accuracy is apparent. The design of such a device has the potential of becoming a standardized means for training medical students since the repeatability of many dysfunctions would be possible. Repeatability is a main concern in real-life medical education situations, because the properties of human soft tissue (stiffness, tenderness etc.) can alter when it is touched by the examiner. The tissue properties are not the same even between the beginning and end of an examination. A legitimate method of evaluating the students would be comparing the first diagnosis of the instructor with the diagnosis of the student. However, when the student takes over the patient, he/she tries to diagnose movement patterns and/or the tissue properties that have already been changed due to the stimulation of the instructor.

The role of simulation in medical education is rapidly increasing. The simulations to train nurses, veterinarians and doctors (osteopathic and allopathic) have been and are still being developed due to their effectiveness and cost-reducing advantages. These simulations can be computer-based or in the form of mannequins that can simulate some functions of the real human body such as breathing, blood pressure, etc. Computer-based haptic simulations require the utilization of a

haptic interface to interact with the virtual objects inside a computer screen. That is clearly not the case when humans really interact with real objects. For instance, the VHB (Williams et al., 2004), the only simulation that is being used to improve palpatory skills of medical students, simulates somatic dysfunctions by increased stiffness of an area on the virtual back and the users "touch" the back with PHANToM® haptic devices which only stimulate the proprioceptive receptors and introduces an extra layer of disturbance between the fingers and the computer-generated objects to be sensed. Therefore, a simulation system which allows the user to interact with a real object would be a better and more effective approach.

The robotic spine concept has been studied over the past years (Mizuuchi et al., 2001, 2002 - Roos et al. 2006). Most of these studies built humanoid robots with a flexible spine which would enhance the human-like movements of the robots and increase the range of movement of the robot's torso. These humanoid robots dealt with the movement of the whole spine, rather than the relative position and stiffness of a vertebra with respect to the adjacent ones. They sufficiently accomplished flexible spine movements with less than the total number of vertebrae in a human spine. However, no research has yet been completed on the subject of developing a robotic spine with anatomically accurate vertebrae geometry and movements for tactile medical education and/or proficiency assessment.

In this paper, kinematic and pseudostatic analyses of a robotic lumbar spine are presented. Simulations are also presented for flexion, extension, right axial rotation and right lateral bending based on the derived pseudostatic model. In the RLS, individual vertebra will be controlled by four cables that are attached to four motors. In this case, a cable-actuated robot is practical due to the space limitations between vertebrae. The robot will be controlled by a joystick or autonomously by preprogramming. The user will interact by touching the posterior aspect of the lumbar spine that is covered with a skin-like material. The user will try to find the type and region of the dysfunction by comparing the movement pattern at different configuration of the robotic lumbar spine.

2. CONSTRUCTION OF RLS GEOMETRY

The geometry of the lumbar spine is constructed using dimensions from previously published experimental data (see Appendix). The parameters that are used in the calculations are shown in Figure 1.

All parameters except for the *facet plane* and *facet plane angle* (∅) have been previously used in the literature and measured to define the morphology of the vertebrae. The facet plane, assuming sagittal symmetry, is defined as the plane that connects the centers of the facets (left/right, superior/inferior) of a vertebra. This plane (manufactured as a plate) will allow us to attach posterior elements with various dimensions on the same vertebra making the system modular. The facet plane angle is defined to be the angle between the facet plane and the posterior wall of the vertebral body. In modeling, a cylindrical shape is assumed for the vertebral bodies. Figure 2 shows the facet plane angle and the approximation of the vertebral bodies as cylinders.

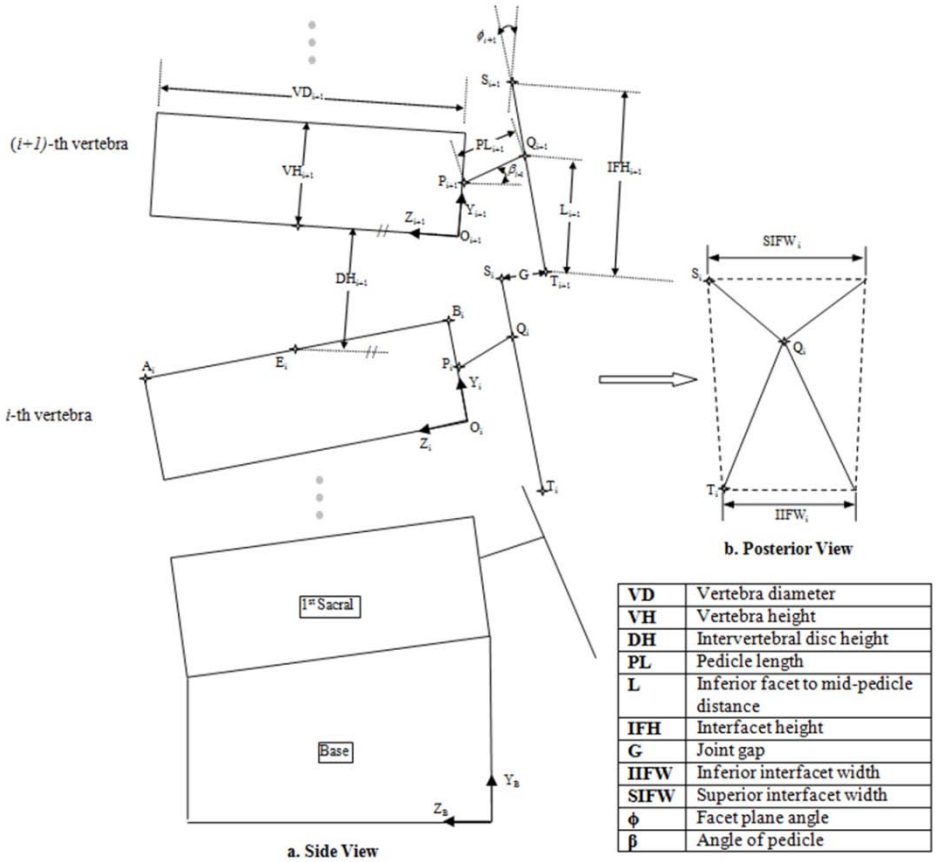

VD	Vertebra diameter
VH	Vertebra height
DH	Intervertebral disc height
PL	Pedicle length
L	Inferior facet to mid-pedicle distance
IFH	Interfacet height
G	Joint gap
IIFW	Inferior interfacet width
SIFW	Superior interfacet width
ϕ	Facet plane angle
β	Angle of pedicle

Figure 1 Lumbar Spine Parameters

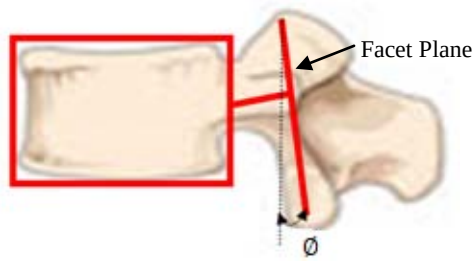

Figure 2 Facet Plane and Angle

The facet plane angles for each vertebra must be calculated in order to fully describe the geometry. Therefore, three unknowns per vertebra are specified including the previously defined facet plane angle (Ø). Two extra unknowns (IIFW and L) are introduced to give us the flexibility to combine parameters obtained from different sources (previously published studies) provided that they are within accepted ranges for a human vertebra. In order to solve for these three unknowns, the distance vector from the origin of a local vertebral frame ($\mathbf{O}_i$ in Figure 1) to the inferior facet center of the upper vertebra ($\mathbf{T}_{i+1}$ in Figure 1) is defined using two different paths. The first path goes through the origin of the upper vertebral frame and upper vertebra's posterior elements (Eq. 1a), whereas the second path follows the current vertebra's posterior elements (Eq. 1b). Equations (1a) and (1b), proceeding from the first sacral vertebra (S1) to the first lumbar vertebra (L1), are solved simultaneously to calculate Ø, IIFW and L at each level of the lumbar spine.

$$ {}^{i}(\mathbf{O}_i\mathbf{T}_{i+1}) = {}^{i}(\mathbf{O}_i\mathbf{O}_{i+1}) $$

$$ + {}_{i+1}^{i}\mathrm{R}\left({}^{i+1}(\mathbf{O}_{i+1}\mathbf{P}_{i+1}) + {}^{i+1}(\mathbf{P}_{i+1}\mathbf{Q}_{i+1}) + {}^{i+1}(\mathbf{Q}_{i+1}\mathbf{T}_{i+1})\right) \quad (1a) $$

$$ {}^{i}(\mathbf{O}_i\mathbf{T}_{i+1}) = {}^{i}(\mathbf{O}_i\mathbf{P}_i) + {}^{i}(\mathbf{P}_i\mathbf{Q}_i) + {}^{i}(\mathbf{Q}_i\mathbf{S}_i) + {}^{i}(\mathbf{S}_i\mathbf{T}_{i+1}) \quad (1b) $$

Where ${}^{i}(\mathbf{S}_i\mathbf{T}_{i+1}) = \mathrm{G}\ {}^{i}(\widehat{\mathbf{SN}})$, G=2mm (Carrera et al., 1979) is the joint gap between the superior facets that make up the facet joints, ${}^{i}(\widehat{\mathbf{SN}})$ is the surface normal vector of the superior facet of the *i*-th vertebra and ${}_{i+1}^{i}\mathrm{R}$ is the rotation matrix which describes the orientation of frame {i+1} with respect to frame {i}. Surface normals for the facets are calculated from the "card angles" as given in Panjabi et al. (1993).

Note that when Eq. (1) is applied to S1 and L5, five unknowns are obtained: Ø, IFW, L for L5 and Ø, L for S1. In order to be able to get these five parameters, two of the unknowns are assumed or iteratively found in either L5 or S1 so that three equations with three unknowns for each vertebra are obtained proceeding towards the uppermost vertebra (L1). The facet plane angle of S1 ($\emptyset_{S1}$) doesn't affect any of the unsolved parameters since the facet centers are points in space and the joint gap (G) does not change with changing α_{S1}. Therefore, inferior facet to mid-pedicle distance of L5 (L_{L5}) is iteratively solveed for until it is the average of L_{L4} and L_{S1} (upper and lower vertebrae) and α_{S1} is the average of all of the facet plane angles above S1. The constructed lumbar spine is shown in Figure 3.

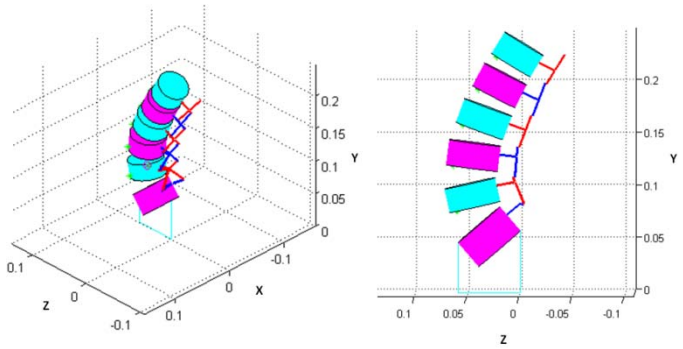

a. 3D View **b. Side View**

Figure 3 Lumbar Spine Geometry

3. RLS KINEMATICS

The robotic spine was designed mainly based on the study by Panjabi et al. (1994) since it details how lumbar spine moves in pre-specified loading conditions. In the related study, the upper-most vertebrae of freshly-frozen cadaveric human lumbar spines with no abnormalities were exposed to external pure moments in order to induce motion and both rotational and translational movement of each vertebra were recorded.

Figure 4 shows the kinematic diagram for the robotic lumbar spine. It is actuated by 20 cables connected to electric motors. Every vertebra is connected to the neighboring vertebrae by spherical joints. The use of spherical joints is intentional since it has been shown that the rotational motion of the vertebrae is more prominent as compared to their translational motion (Panjabi et al., 1994). The location of the spherical joint for each vertebra is at the inferoposterior corner in the mid-sagittal plane of the vertebral body as shown in Figure 4. These locations correspond to the origin of the coordinate frames with respect to which the angles of rotation were recorded in Panjabi et al. (1994). As discussed previously, the facet plane in Figure 4 is designed to be used as the base on which posterior elements with various dimensions can be attached.

The cable connection points on the ground are at the corners of five trapezoids (Figure 5). The innermost trapezoid that includes the connection points for the fifth lumbar vertebra (L5) has posterior base length of 0.4m, anterior base length of 0.2m and height of 0.15m. The remaining four trapezoids are constructed with increasing the height of the adjacent (inner) one by 0.05m anteriorly and 0.05m posteriorly. This placement of the cable connections on the ground prevented cable interference during the simulations (see Section 5. SIMULATION EXAMPLES).

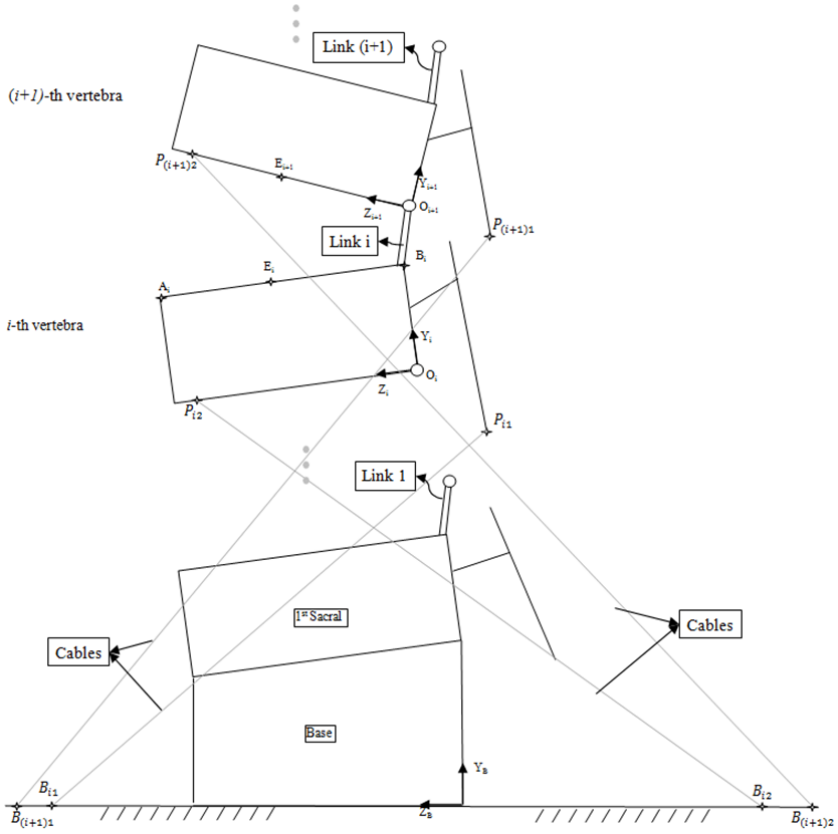

a. Side View

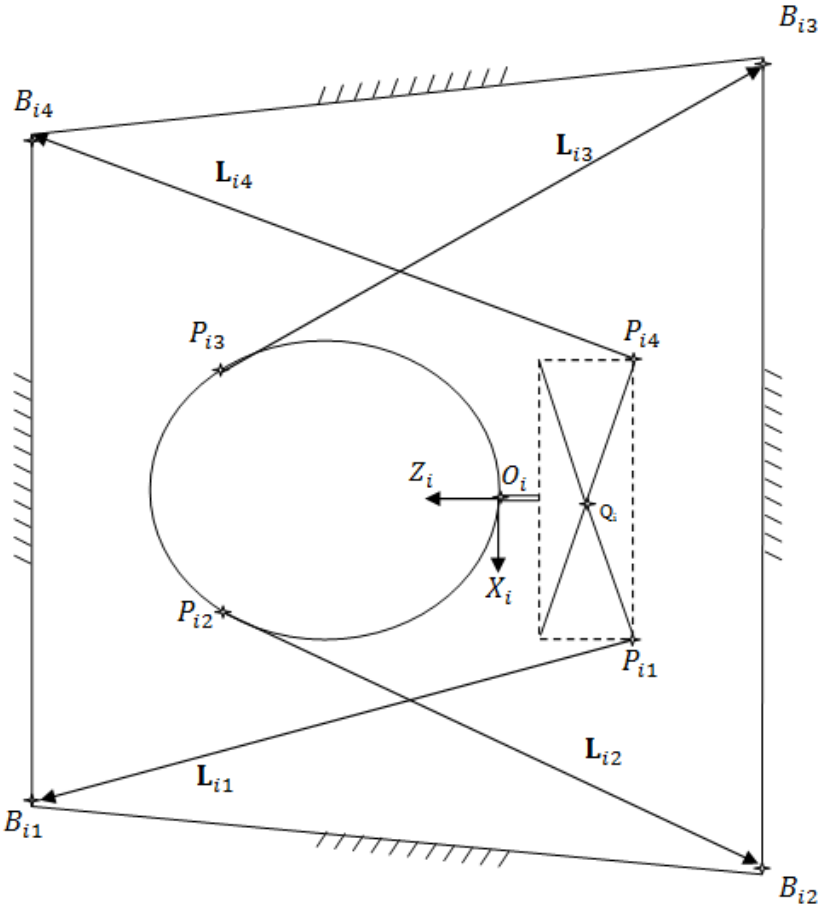

b. Top View

Figure 4 Robotic Lumbar Spine Kinematics Diagram

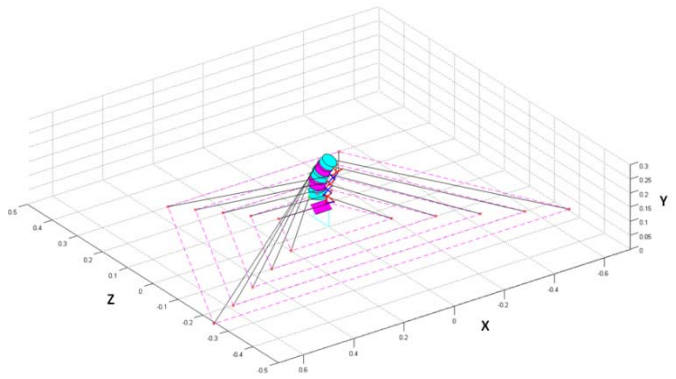

Figure 5 Robotic Lumbar Spine with Cables

3.1 RLS Inverse Kinematics

Inverse pose kinematics is relatively straight forward for parallel manipulators as compared to serial. The problem statement is as follows: "Given the final pose for each vertebra, $\left[{}^{i}_{i+1}T\right]$, calculate 20 active cable lengths L_{ij} (i = 1, …, 5 and j = 1, …, 4)". Notice that since a vertebra has only three degrees of freedom (rotations), the inverse kinematics problem, in this case, may also be constructed to find the rotation matrices of individual vertebra with respect to their neighbor (lower vertebra). The cable connection points on the vertebra in the base frame {B} are:

$$\begin{aligned}
\left\{{}^{B}\mathbf{P}_{i1}\right\} &= \left[{}^{B}_{i}T\right]\left\{{}^{i}\mathbf{P}_{i1}\right\} \qquad i = 1,2,3,4,5\\
\left\{{}^{B}\mathbf{P}_{i2}\right\} &= \left[{}^{B}_{i}T\right]\left\{{}^{i}\mathbf{P}_{i2}\right\}\\
\left\{{}^{B}\mathbf{P}_{i3}\right\} &= \left[{}^{B}_{i}T\right]\left\{{}^{i}\mathbf{P}_{i3}\right\}\\
\left\{{}^{B}\mathbf{P}_{i4}\right\} &= \left[{}^{B}_{i}T\right]\left\{{}^{i}\mathbf{P}_{i4}\right\}
\end{aligned} \tag{2}$$

Where the 4x4 transformation matrix that represents i-th vertebra coordinate system with respect to the base frame {B} is $[{}^{B}_{i}T] = [{}^{B}_{1}T][{}^{1}_{2}T]\cdots[{}^{i-1}_{i}T]$. The connection points of the cables, $\left\{{}^{i}\mathbf{P}_{i1}\right\}, \left\{{}^{i}\mathbf{P}_{i2}\right\}, \left\{{}^{i}\mathbf{P}_{i3}\right\}, \left\{{}^{i}\mathbf{P}_{i4}\right\}$, on the vertebra are constant and known, from vertebra geometry, with respect to local vertebra coordinate frame, $\{i\}$. Given these cable connection points on the vertebrae and the ground (B_{i1}, B_{i2}, B_{i3}, B_{i4}), the cable lengths are found as follows:

$$\begin{aligned}
L_{i1} &= \|\mathbf{L}_{i1}\| = \left\|{}^{B}\mathbf{B}_{i1} - {}^{B}\mathbf{P}_{i1}\right\| \quad L_{i2} = \|\mathbf{L}_{i2}\| = \left\|{}^{B}\mathbf{B}_{i2} - {}^{B}\mathbf{P}_{i2}\right\|\\
L_{i3} &= \|\mathbf{L}_{i3}\| = \left\|{}^{B}\mathbf{B}_{i3} - {}^{B}\mathbf{P}_{i3}\right\| \quad L_{i4} = \|\mathbf{L}_{i4}\| = \left\|{}^{B}\mathbf{B}_{i4} - {}^{B}\mathbf{P}_{i4}\right\|
\end{aligned} \tag{3}$$

3.2 RLS Forward Pose Kinematics

Forward pose kinematics problem is stated as follows: "Given the 20 active cable lengths L_{ij} (i = 1, …, 5 and j = 1, …, 4), calculate the final pose, $\left[{}^{i}_{i+1}T\right]$ ". The forward kinematics solution for cable suspended robots is not as straight-forward as the inverse pose kinematics solution. The final pose can be described as:

$$\left[{}^{i}_{i+1}T\right]_{4x4} = \begin{bmatrix} \left[{}^{i}_{i+1}R\right]_{3x3} & \left\{{}^{i}\mathbf{P}_{(i+1)ORG}\right\}_{3x1} \\ 0 \quad 0 \quad 0 & 1 \end{bmatrix} \tag{4}$$

where ${}^{i}\mathbf{P}_{(i+1)ORG}$, known from the dimensions of the vertebrae, is the position vector from the origin of {i} to the origin of {i+1} in frame {i} and $\left[{}^{i}_{i+1}R\right]$ is the rotation matrix which describes the orientation of frame {i+1} with respect to frame {i}, using X-Y-Z (α, β, γ) Euler angles:

$${}^{i}_{i+1}R = \begin{bmatrix} c\beta c\gamma & -c\beta s\gamma & s\beta \\ s\alpha s\beta c\gamma + c\alpha s\gamma & -s\alpha s\beta s\gamma + c\alpha c\gamma & -s\alpha c\beta \\ -c\alpha s\beta c\gamma + s\alpha s\gamma & c\alpha s\beta s\gamma + s\alpha c\gamma & c\alpha c\beta \end{bmatrix} \tag{5}$$

Where $c\alpha = \cos\alpha$, $c\beta = \cos\beta$, $c\gamma = \cos\gamma$, $s\alpha = \sin\alpha$ $s\beta = \sin\beta$, $s\gamma = \sin\gamma$.

The rotation angles are solved by using the following vector loop closure equations for the cable lengths:

$$\begin{aligned}
\left\|\left({}^{B}\boldsymbol{O}_{i} - {}^{\boldsymbol{B}}\boldsymbol{B}_{i1}\right) + \left[{}^{B}_{i}R\right]\left\{{}^{i}\boldsymbol{P}_{i1}\right\}\right\| &= \|\boldsymbol{L}_{i1}\| = L_{i1}\\
\left\|\left({}^{B}\boldsymbol{O}_{i} - {}^{\boldsymbol{B}}\boldsymbol{B}_{i2}\right) + \left[{}^{B}_{i}R\right]\left\{{}^{i}\boldsymbol{P}_{i2}\right\}\right\| &= \|\boldsymbol{L}_{i2}\| = L_{i2}\\
\left\|\left({}^{B}\boldsymbol{O}_{i} - {}^{\boldsymbol{B}}\boldsymbol{B}_{i3}\right) + \left[{}^{B}_{i}R\right]\left\{{}^{i}\boldsymbol{P}_{i3}\right\}\right\| &= \|\boldsymbol{L}_{i3}\| = L_{i3}\\
\left\|\left({}^{B}\boldsymbol{O}_{i} - {}^{\boldsymbol{B}}\boldsymbol{B}_{i4}\right) + \left[{}^{B}_{i}R\right]\left\{{}^{i}\boldsymbol{P}_{i4}\right\}\right\| &= \|\boldsymbol{L}_{i4}\| = L_{i4}
\end{aligned} \tag{6}$$

The existence of transcendental functions in the equations makes them nonlinear. Therefore, the Newton-Raphson method is used to solve the system of nonlinear equations iteratively. The method is based on the linear approximation of the functions by using the Taylor series expansion and solving these equations for the change in the independent variables. The steps are:

- Initial guess for $\boldsymbol{X}_k = \{\alpha \ \beta \ \gamma\}^T$
- Find $\Delta\boldsymbol{X}_k = \{\Delta\alpha \ \Delta\beta \ \Delta\gamma\}^T$

$$\{F_i(\boldsymbol{X})\}_{4x1} + [J]_{4x3}\{\Delta\boldsymbol{X}\}_{3x1} = \{0\}_{4x1}$$
$$\{\Delta\boldsymbol{X}\} = -[J]^{+}\{F_i(\boldsymbol{X})\}$$

Where:

$$F_i(\boldsymbol{X}) = \{f_1(\boldsymbol{X}) \ f_2(\boldsymbol{X}) \ f_3(\boldsymbol{X}) \ f_4(\boldsymbol{X})\}^T$$
$$J = \begin{bmatrix} \frac{\partial f_1}{\partial\alpha} & \frac{\partial f_1}{\partial\beta} & \frac{\partial f_1}{\partial\gamma} \\ \vdots & \vdots & \vdots \\ \frac{\partial f_4}{\partial\alpha} & \frac{\partial f_4}{\partial\beta} & \frac{\partial f_4}{\partial\gamma} \end{bmatrix}$$

- Get the improved estimate, $\boldsymbol{X}_{k+1} = \boldsymbol{X}_k + \Delta\boldsymbol{X}_k$
- Stop when $\|\Delta X_k\| \le Tol$, where Tol is a pre-specified tolerance value.

Where $[J]^{+} = ([J]^T[J])^{-1}[J]^T$ is the pseudoinverse of the overconstrained Jacobian matrix and $F_i(\boldsymbol{X})$ is composed of:

$$\begin{aligned}
f_1(\boldsymbol{X}) &= \left\|\left({}^{B}\boldsymbol{O}_{i} - {}^{\boldsymbol{B}}\boldsymbol{B}_{i1}\right) + \left[{}^{B}_{i}R\right]\left\{{}^{i}\boldsymbol{P}_{i1}\right\}\right\| - L_{i1}\\
f_2(\boldsymbol{X}) &= \left\|\left({}^{B}\boldsymbol{O}_{i} - {}^{\boldsymbol{B}}\boldsymbol{B}_{i2}\right) + \left[{}^{B}_{i}R\right]\left\{{}^{i}\boldsymbol{P}_{i2}\right\}\right\| - L_{i2}\\
f_3(\boldsymbol{X}) &= \left\|\left({}^{B}\boldsymbol{O}_{i} - {}^{\boldsymbol{B}}\boldsymbol{B}_{i3}\right) + \left[{}^{B}_{i}R\right]\left\{{}^{i}\boldsymbol{P}_{i3}\right\}\right\| - L_{i3}\\
f_4(\boldsymbol{X}) &= \left\|\left({}^{B}\boldsymbol{O}_{i} - {}^{\boldsymbol{B}}\boldsymbol{B}_{i4}\right) + \left[{}^{B}_{i}R\right]\left\{{}^{i}\boldsymbol{P}_{i4}\right\}\right\| - L_{i4}
\end{aligned} \tag{7}$$

Notice that, as shown by the equation below, ${}^{B}\boldsymbol{O}_i$ simply consists of the first three rows of the last column of the homogenous transformation matrix ${}^{B}_{i}T$. It is the position vector from the origin of the base frame to the origin of the local frame on *i*-th vertebra and referenced to the base frame.

$$\left\{ {}^{B}\boldsymbol{O}_i \right\} = [{}^{B}_{i}T]\left\{ {}^{i}\boldsymbol{O}_i \right\} = [{}^{B}_{i}T]\{0\ 0\ 0\ |1\}^T$$

4. RLS PSEUDOSTATICS

In this section, pseudostatic modeling of the robotic lumbar spine is presented. The free-body diagram of a vertebra is shown in Figure 6.

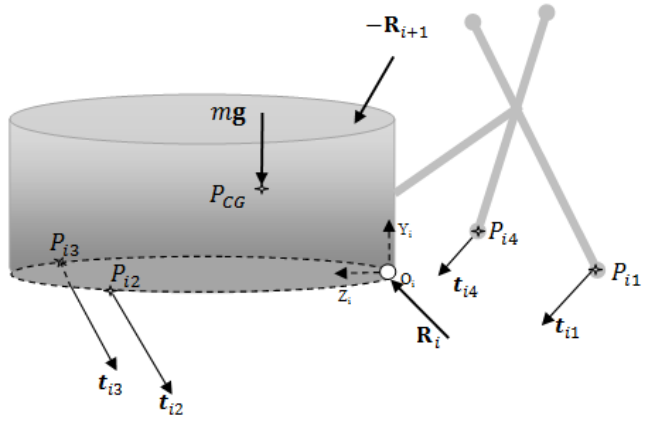

Figure 6 Vertebra Free-Body Diagram

The static force and moment (about the origins of the local vertebra frames) equilibrium equations are:

$$\begin{aligned} &\sum_{j=1}^{4} \mathbf{t}_{ij} + m_i\, {}^{B}\mathbf{g} + {}^{B}\mathbf{R}_i - {}^{B}\mathbf{R}_{i+1} = \mathbf{F}_R \qquad i = 1,2,3,4,5 \\ &\sum_{j=1}^{4} \mathbf{m}_{ij} + {}^{B}_{i}R\ {}^{i}\mathbf{P}_{CG} \times m_i\, {}^{B}\mathbf{g} - {}^{B}_{i}R\ {}^{i}\mathbf{P}_S \times {}^{B}\mathbf{R}_{i+1} = \mathbf{M}_R \end{aligned} \tag{8}$$

where m_i is the mass of the vertebra, $\mathbf{t}_{ij} = t_{ij}\,\hat{\mathbf{L}}_{ij}$ is the tension vector with magnitude t_{ij} and in the direction of $\hat{\mathbf{L}}_{ij}$, i.e. the unit vector on cable j of i^{th} vertebra (i = 1,…,5 and j = 1,2,3,4). ${}^{B}\mathbf{g} = \{0\ -9.81\ 0\}^{\mathrm{T}}$ is the gravity vector in {B}. ${}^{B}\mathbf{R}_i = \{R_x\ R_y\ R_z\}^T$ is the reaction force at the ball of the *i*-th vertebra's ball and socket joint. Notice that $-{}^{B}\mathbf{R}_{i+1}$ is the reaction force at the ball of the *(i+1)*-th neighboring vertebra in the opposite direction. $\mathbf{m}_{ij} = {}^{B}_{i}R\ {}^{i}\mathbf{P}_{ij} \times \mathbf{t}_{ij}$ is the moment due to the tension on cable *j* of *i*-th vertebra where ${}^{i}\mathbf{P}_{ij}$ is the moment arm from the origin of the local vertebral frame $\{i\}$ to the connection point of the same cable on that vertebra. ${}^{i}\mathbf{P}_{CG}$ and ${}^{i}\mathbf{P}_S$ are the position vectors from the local origin to the center of gravity and center of the socket in $\{i\}$, respectively. $\mathbf{F}_R$ and $\mathbf{M}_R$ compose the wrench that is exerted on the environment by that particular vertebra.

In this part of the analysis, however, it is not intended to analyze the reaction forces at the ball and socket joints. It is rather intended to relate positive cable tensions to a given configuration. Therefore, static equilibrium of the entire structure is considered with respect to base frame to eliminate the action-reaction pairs from the equations. In this case, the equations of static equilibrium for the structure are written as:

$$\begin{aligned} &\sum_{i=1}^{N_v}\sum_{j=1}^{N_c} \mathbf{t}_{ij} + \sum_{i=1}^{N_v}(m_i\, {}^{B}\mathbf{g}) + \mathbf{R}_{\mathrm{G}} = \sum_{i=1}^{N_v}(\mathbf{F}_{\mathrm{R}})_{\mathrm{i}} \\ &\sum_{i=1}^{N_v}\sum_{j=1}^{N_c} \mathbf{m}_{ij} + \sum_{i=1}^{N_v}\left(\left({}^{B}_{i}R\ {}^{i}\mathbf{P}_{CG} + {}^{B}\boldsymbol{P}_{iORG}\right) \times m_i\, {}^{\mathrm{B}}\mathbf{g}\right) + \mathbf{M}_{\mathbf{G}} = \sum_{i=1}^{N_v}(\mathbf{M}_{\mathrm{R}})_{\mathrm{i}} \end{aligned} \tag{9}$$

where $\mathbf{R}_{\mathrm{G}}$ and $\mathbf{M}_{\mathrm{G}}$ are, respectively, the ground reaction forces and moments on the base of the structure. . N_v(=5) is the total number of vertebrae and N_c(=4) is the number of cables per vertebra. The moment due to cable tensions now needs to be calculated as $\mathbf{m}_{ij} = \left({}^{B}_{i}R\ {}^{i}\mathbf{P}_{ij} + {}^{B}\boldsymbol{P}_{iORG}\right) \times \mathbf{t}_{ij}$. The equations in (9) can be rearranged in matrix form as follows:

$$[\mathbf{S}]\{\mathbf{t}\} + \{\mathbf{f}_{\mathrm{G}}\} = \{\mathbf{W}_{\mathbf{R}} - \mathbf{G}_{\mathbf{R}}\} \tag{10}$$

where $\{\mathbf{t}\}_{20\mathrm{x}1} = \{\mathrm{t}_{11}\ \mathrm{t}_{12}\ \mathrm{t}_{13}\ \mathrm{t}_{14}\ \cdots\ \mathrm{t}_{51}\ \mathrm{t}_{52}\ \mathrm{t}_{53}\ \mathrm{t}_{54}\}^{\mathrm{T}}$ is the active cable tension magnitudes, $\{\mathbf{W}_{\mathbf{R}}\}_{6\mathrm{x}1} = \{\mathbf{F}_{\mathbf{R}}\ \mathbf{M}_{\mathbf{R}}\}^{\mathrm{T}}$ is the cumulative external wrench vector exerted on the environment by the structure, $\{\mathbf{G}_{\mathbf{R}}\}_{6\mathrm{x}1} = \left\{\sum_{i=1}^{N_v}(m_i\, {}^{B}\mathbf{g})\ \ \sum_{i=1}^{N_v}\left(\left({}^{B}_{i}R\ {}^{i}\mathbf{P}_{CG} + {}^{B}\boldsymbol{P}_{iORG}\right) \times m_i\, {}^{\mathrm{B}}\mathbf{g}\right)\right\}^{\mathrm{T}}$ is the gravity loading wrench vector, $\{\mathbf{f}_{\mathrm{G}}\}_{6\mathrm{x}1}$=$\{\mathbf{R}_{\mathrm{G}}\ \mathbf{M}_{\mathrm{G}}\}^{\mathrm{T}}$ is the ground reaction vector and $[\mathbf{S}]_{6\mathrm{x}20}$ is defined as:

$$[\mathbf{S}] = \begin{bmatrix} \hat{\boldsymbol{L}}_{11} & \cdots & \hat{\boldsymbol{L}}_{54} \\ -\hat{\boldsymbol{L}}_{11} \times \left({}^{B}_{1}R\ {}^{1}\mathbf{P}_{11} + {}^{B}\boldsymbol{P}_{1ORG}\right) & \cdots & -\hat{\boldsymbol{L}}_{54} \times \left({}^{B}_{5}R\ {}^{5}\mathbf{P}_{54} + {}^{B}\boldsymbol{P}_{5ORG}\right) \end{bmatrix}$$

5. SIMULATION EXAMPLES

The pseudostatic simulations were run for flexion, extension, right lateral bending and right axial rotation for 10 seconds. In this section, results are presented for only flexion due to space limitations. The vertebrae were assigned their final orientations (Figure 7) when they were exposed to the maximum moment (10N.m) about the corresponding axis in Panjabi et al. (1994). The positive cable tensions (Figure 8) in Eq. (10) and corresponding ground reactions (Figure 9) were found by using MATLAB's built-in function *lsqnonlin*() which solves the non-linear least squares problem.

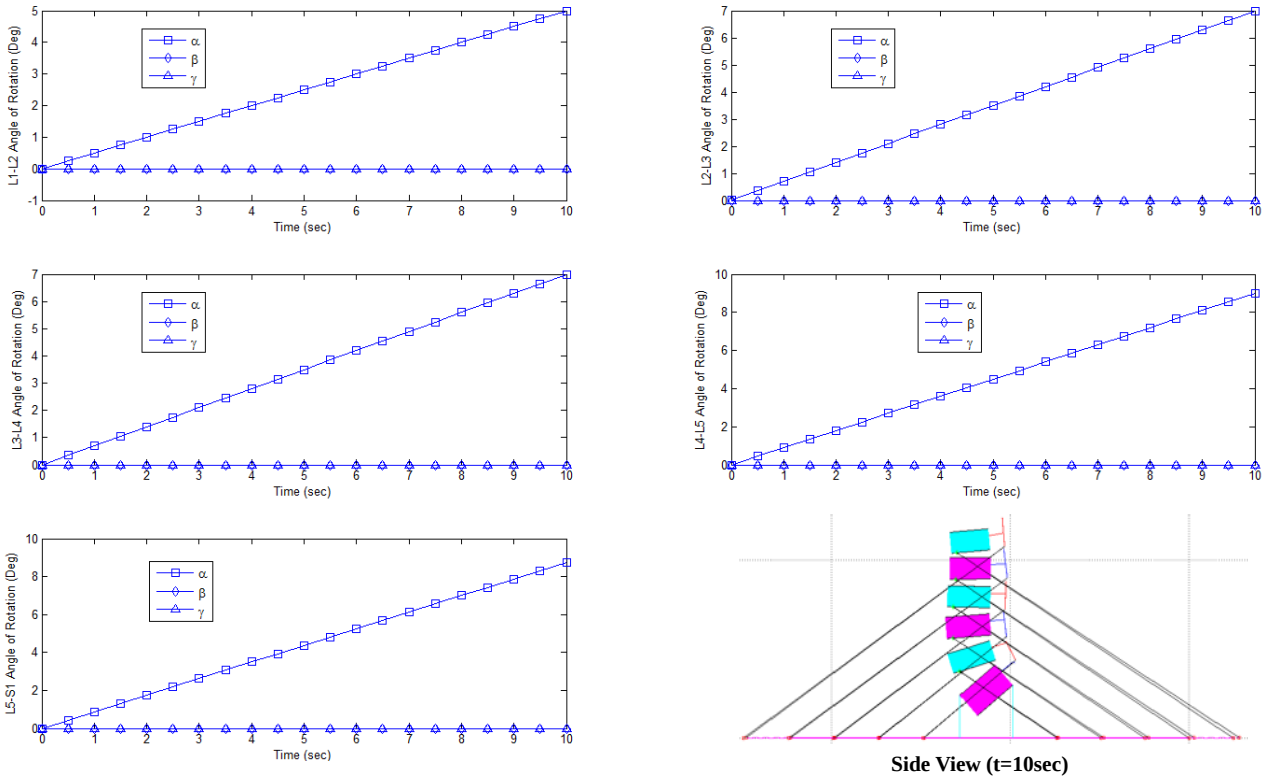

Figure 7 Simulated Angles of Rotation for Flexion

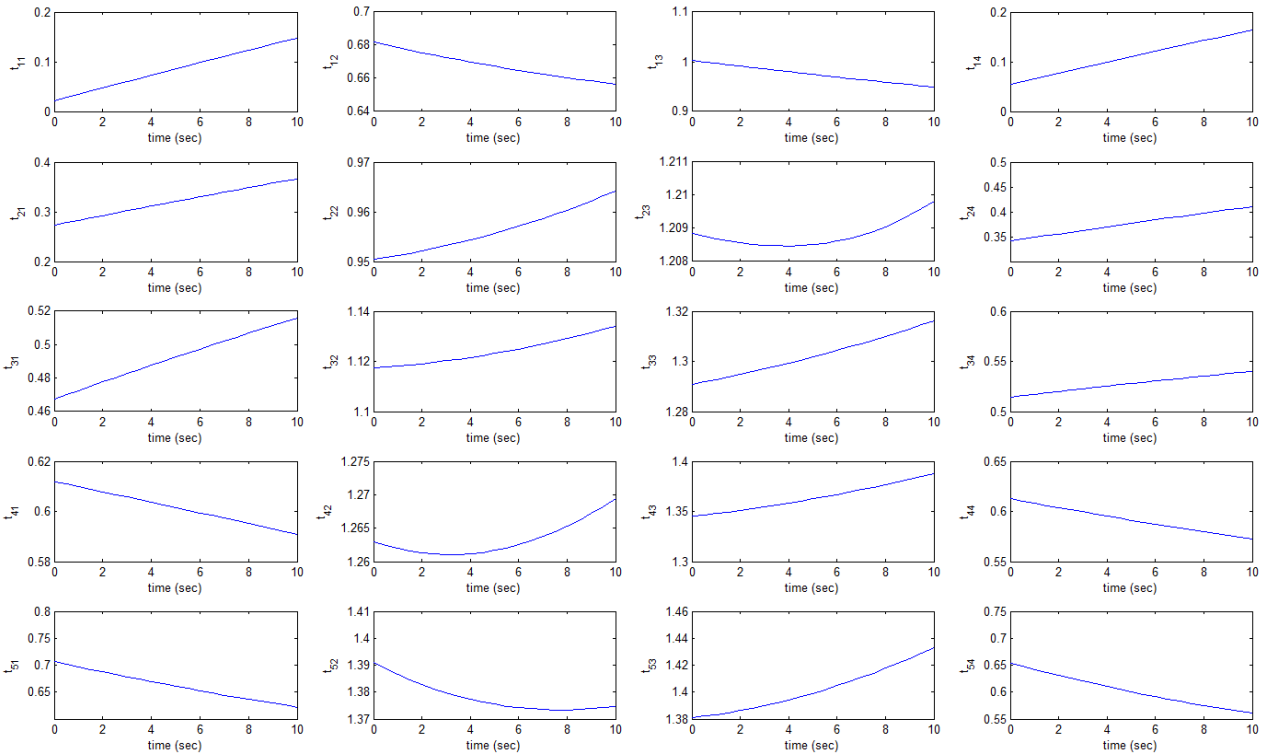

Figure 8 Cable Tensions (N) for Flexion

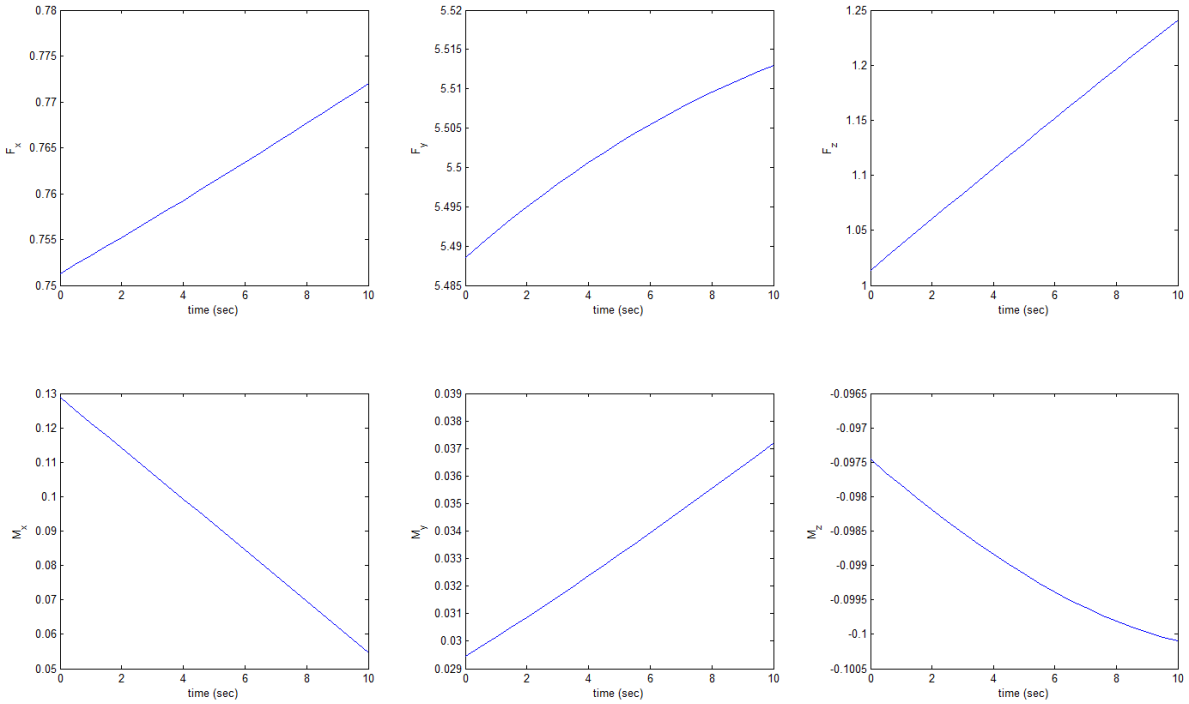

Figure 9 Ground Reactions (N and Nm) for Flexion

As in any cable-actuated robot, maintaining positive cable tensions at all times is one of the main challenges since the cables can only pull, but not push. The simulations for RLS revealed that positive cable tensions can be maintained at any orientation during the simulation under the pseudostatic motion assumption.

The simulations including flexion, extension, right lateral bending and right axial rotation also confirmed that the selected connection points on the ground and on the vertebrae prevented any cable interference. These connection points that are arranged as the corners of trapezoids will also enable easy access to the posterior elements of the vertebrae during training.

6. CONCLUSION

In this paper, the cable-actuated robotic lumbar spine (RLS) concept was introduced and kinematic and pseudostatic analyses of the robot were presented. The design purpose of RLS is to provide medical students with a better way to practice palpation of the lumbar spine. RLS can be programmed to simulate normal and abnormal movement patterns of the spine representing various dysfunctions such as stiff vertebral joints, facet fusion etc.

Future work plans include developing dynamic equations of motion of the RLS in order to design a nonlinear robust controller. Even though the patients' movements during diagnoses may be slow enough to ignore inertial effects, the RLS will be designed to follow a wide range of trajectories with different velocity and acceleration constraints.

REFERENCES

Bernhardt M, Bridwell K, 1989, "Segmental Analysis of the Sagittal Plane Alignment of the Normal Thoracic and Lumbar Spines and Thoracolumbar Junction", *Spine*, 14(7):717-721.

Carrera GF, Haughton VM, Syvertsen A, Williams AL, 1979, "Computed tomography of the lumbar facet joints", *Radiology*, 134:145-148.

Marchesi D, Schneider E, Glauser P, Aebi M, 1988, "Morphometric analysis of the thoracolumbar and lumbar pedicles, anatomo-radiologic study", *Surgical Radiologic Anatomy*, 10:317-322.

Marty C, Boisaubert B, Descamps H, Montigny JP, Hecquet J, Legaye J, Duval-Beaupere G, 2002, "The sagittal anatomy of the sacrum among young adults, infants, and spondylolisthesis patients", European Spine Journal, 11(2):119-125.

Mizuuchi I, Inaba M, Inoue H, 2001, "Flexible spine human-form robot-development and control of the posture of the spine", IEEE/RSJ International Conference on Intelligent Robots and Systems.

Mizuuchi I, Tajima R, Yoshikai T, Sato D., Nagashima K., Inaba M., Kuniyoshi Y., Inoue H., 2002**, "**The design and

control of the flexible spine of a fully tendon-driven humanoid "Kenta"", IEEE/RSJ International Conference on Intelligent Robots and Systems.

Panjabi MM, Goel V, Oxland T, Takata K, Duranceau J, Krag M, Price M. , 1992, "Human lumbar vertebrae. Quantitative three-dimensional anatomy", *Spine*, 17(3):299-306.

Panjabi MM, Oxland T, Takata K, Goel V, Duranceau J, Krag M, 1993, "Articular facets of the human spine. Quantitative three-dimensional anatomy", *Spine*, 18(10):1298-310.

Panjabi MM, Oxland TR, Yamamoto I, Crisco JJ, 1994, "Mechanical behavior of the human lumbar and lumbosacral spine as shown by three-dimensional load-displacement curves", *J Bone Joint Surg Am.*, 76:413-424.

Roos L, Guenter F, Guignard A, Billard AG, 2006, "Design of a Biomimetic Spine for the Humanoid Robot Robota", IEEE / RAS-EMBS International Conference on Biomedical Robotics and Biomechatronics, Pisa, Italy.

Todd TW, Pyle IS, 1928, "A quantitative study of the vertebral column by direct and roentgenoscopic methods", *American Journal of Physical Anthropology*, 12(2):321:338.

Williams II RL, Srivastava M , Howell JN, Conatser RR , Eland DC, Burns JM, and Chila AG , 2004, The Virtual Haptic Back for Palpatory Training, Sixth International Conference on Multimodal Interfaces, State College, PA, October 13-15.

APPENDIX

Dimensions used to construct the lumbar spine geometry

Table 1 Pedicle Length and Angle (Marchesi et al., 1988)[*]

	PL (mm)	β°
L1	16.8	5.2
L2	16.8	2.2
L3	17.0	0.8
L4	16.3	0.1
L5	17.7	-1.4

[*] Along sagittal projection, from posterior aspect of the transverse process to the attachment of the pedicle to the vertebral body

Table 2 Vertebra height and diameter (Panjabi et al., 1992)

	VH (mm)	VD (mm)
L1	23.8	43.3
L2	24.3	45.5
L3	23.8	48.0
L4	24.1	49.5
L5	22.9	49.4

Table 3 Interfacet Height and Superior Interfacet Width (Panjabi et al., 1993)

	IFH (mm)	SIFW (mm)
L1	32.15	26.20
L2	32.70	26.40
L3	32.00	28.60
L4	28.40	31.40
L5	26.25	35.00

Table 4 Disc Height (Todd and Pyle, 1928)

	DH (mm)
L1	9.95
L2	11.45
L3	12.25
L4	14.75
L5	17.30

Table 5 Left Superior Facet Normals[ψ] (calculated from Panjabi et al., 1993)

	x	y	z
L1	-0.73261	0.13744	-0.66663
L2	-0.73828	0.09150	-0.66826
L3	-0.67310	0.12187	-0.72944
L4	-0.53250	0.15212	-0.83265
L5	-0.48030	0.07759	-0.87366
S1	-0.59614	0.23684	-0.76715

[ψ] Right superior facet normals are found by using sagittal (*y*-*z* plane) symmetry

Table 6 Sagittal angulations of Normal Lumbar Curve (Bernhardt et al., 1989)

	(deg)
L1-L2	-4.0
L2-L3	-7.0
L3-L4	-13.0
L4-L5	-20.0
L5-S1	-28.0
Sacral Slope (Marty et al., 2002)	40.59

Parameters solved for the lumbar spine geometry

Table 7 ∅, L and IFW (current study)

	∅°	L (mm)	IIFW (mm)
L1	-0.6268	15.2	23.4
L2	6.4942	16.0	25.9
L3	-0.3603	17.4	29.3
L4	2.4798	19.2	33.1
L5	9.9356	23.9	38.2
S1	3.5845	28.7	N/A[†]

[†] Not needed in order to define the lumbar spine geometry